This is the accepted version of Jeona J.S., Bersini S., Gilardi M., Dubini G., Charest J.L., Moretti M., Kamm R.D., Human 3D vascularized organotypic microfluidic assays to study breast cancer cell extravasation. PROCEEDINGS OF THE NATIONAL ACADEMY OF SCIENCES OF THE UNITED STATES OF AMERICA, 2015, 112-1: 214-219.
The final publication is available at http://dx.doi.org/10.1073%2Fpnas.1417115112

Human 3D vascularized organotypic microfluidic assays to study breast cancer cell extravasation

Jessie S. Jeon[a,1], Simone Bersini[b,c,1], Mara Gilardi[c,d], Gabriele Dubini[e], Joseph L. Charest[f], Matteo Moretti[c,2,3], and Roger D. Kamm[a,g,2,3]

[a]Department of Mechanical Engineering, Massachusetts Institute of Technology, Cambridge, MA 02139; [b]Department of Electronics, Information and Bioengineering, Politecnico di Milano, 20133 Milan, Italy; [c]Cell and Tissue Engineering Laboratory, Istituto di Ricovero e Cura a Carattere Scientifico (IRCCS) Istituto Ortopedico Galeazzi, 20161 Milan, Italy; [d]PhD School in Life Sciences, Department of Biotechnology and Biosciences, University of Milano–Bicocca, 20126 Milan, Italy; [e]Department of Chemistry, Materials and Chemical Engineering, Politecnico di Milano, 20133 Milan, Italy; [f]Charles Stark Draper Laboratory, Cambridge, MA 02139; and [g]Department of Biological Engineering, Massachusetts Institute of Technology, Cambridge, MA 02139

A key aspect of cancer metastases is the tendency for specific cancer cells to home to defined subsets of secondary organs. Despite these known tendencies, the underlying mechanisms remain poorly understood. Here we develop a microfluidic 3D in vitro model to analyze organ-specific human breast cancer cell extravasation into bone- and muscle-mimicking microenvironments through a microvascular network concentrically wrapped with mural cells. Extravasation rates and microvasculature permeabilities were significantly different in the bone-mimicking microenvironment compared with unconditioned or myoblast containing matrices. Blocking breast cancer cell A_3 adenosine receptors resulted in higher extravasation rates of cancer cells into the myoblast-containing matrices compared with untreated cells, suggesting a role for adenosine in reducing extravasation. These results demonstrate the efficacy of our model as a drug screening platform and a promising tool to investigate specific molecular pathways involved in cancer biology, with potential applications to personalized medicine.

microenvironment | breast cancer | metastasis | extravasation | microfluidics

Dissemination of cancer cells from a primary tumor to secondary loci is responsible for more than 90% of cancer-related mortality (1). Despite significant advances in diagnostics and therapy, most of the available treatments are not effective, because the disseminated cells are resistant to conventional agents (2). Invasion and metastasization are complex and multistep processes guided by a wide spectrum of genetic and biochemical determinants (3). A key aspect of metastases is reflected in the interactions between specific cancer cell types and different secondary organs. Although circulatory patterns and flow rates may play some role in cancer cell dissemination, it appears that the organ specificity of metastases is primary due to the cross-talk between specific cancer cells and biologically unique tissues: the seed-and-soil paradigm (4). For example, breast and prostate cancers are known to metastasize frequently to bone (5), with 70% of advanced breast cancer patients affected by skeletal metastases, leading to high rates of morbidity and mortality (6). Moreover, it has been recently demonstrated that breast cancer cells can reseed from bone to other sites including the breast, further emphasizing the key role of the bone microenvironment in the metastatic process (7).

Metastasis organ specificity and extravasation appear to be tightly coupled because specific chemo-attractant molecules are secreted by organ-specific stromal cells (8). Furthermore, positive interactions with circulating noncancer cells, e.g., platelets, leukocytes, and monocytes/macrophages, promote cancer cell transendothelial migration into surrounding tissues (9).

In vivo and ex vivo studies have been performed to investigate cancer cell extravasation in mouse models through liver sinusoids and pulmonary circulation (10) or in zebrafish embryos (11). Recently, Schumacher et al. have shown the influence of platelet-secreted nucleotides playing a crucial role in the transendothelial migration of cancer cells in the lung of mouse models (12). In vivo models have been developed to study breast cancer metastases to bone by means of i.v. and skeletal injection of breast cancer cells in mice (13). Although in vivo models play an essential role in replicating physiological conditions, they lack the possibility to analyze highly specific interactions between human cancer cells, human blood vessels, and tissues, and they are not well suited to perform reproducible parametric studies. To remedy this, several in vitro models have been developed to analyze cell migration mechanisms and particularly the invasive potential of cancer cells (14). However, these models are often highly simplified, such as the Boyden chamber or wound assays (15), which fail to allow the analysis of complex cell–cell and cell–matrix interactions, are limited in their capability to tightly control the local microenvironment, and offer only limited imaging.

Microfluidics overcomes some of the technical limitations of traditional assays (16), allowing the study of cancer metastases under biochemically and biophysically controlled 3D microenvironments coupled with high-resolution real-time imaging (17). Various microfluidic models have been developed for studying tumor angiogenesis (18), transition to invasion (19), intravasation (20), the role of interstitial flow (21) and matrix stiffness (22) on

Significance

The cancer biology seed-and-soil paradigm recognizes the existence of organ-specific patterns of metastasization that drive the spread of selected primary tumors toward specific secondary loci. However, despite efforts to model the organotypic microenvironment, the organ specificity of cancer metastases needs to be elucidated. The relevance of this study lies in the generation of a human vascularized organ-specific microenvironment, which can be used to investigate and tune the extravasation process of metastatic tumor cells. Furthermore, beyond mimicking the pro- or antimetastatic signatures of different microenvironments, our microfluidic model provides insights into different properties of organ-specific endothelia. This study paves the way toward advanced in vitro models to screen for highly tailored organ-specific therapeutics and investigate key molecular pathways involved in organ-specific metastases.

Author contributions: J.S.J., S.B., G.D., J.L.C., M.M., and R.D.K. designed research; J.S.J., S.B., and M.G. performed research; J.S.J., S.B., M.G., M.M., and R.D.K. analyzed data; and J.S.J., S.B., M.M., and R.D.K. wrote the paper.

The authors declare no conflict of interest.

This article is a PNAS Direct Submission.

[1]J.S.J. and S.B. contributed equally to this work.

[2]M.M. and R.D.K. contributed equally to this work.

[3]To whom correspondence may be addressed. Email: matteo.moretti@grupposandonato.it or rdkamm@mit.edu.

This article contains supporting information online at www.pnas.org/lookup/suppl/doi:10.1073/pnas.1417115112/-/DCSupplemental.

cancer cell migration, adhesion (23), and extravasation (24, 25). Recently, our group presented a microfluidic model to investigate the specificity of breast cancer metastasis to bone, providing quantitative data on cancer cell extravasation rate and reproducing the effects of the CXCL5–CXCR2 interaction between bone cells and metastatic breast cancer cells observed in vivo (26). However, in that system, the vascular wall was represented by an endothelial monolayer on the side of a central gel region. With the recent attempts in inducing vasculogenesis (27, 28), vascular networks have been generated inside the gel region either by coculture with human lung fibroblasts in separate gel regions or by interstitial flow. Despite the tremendous advances in modeling angiogenesis and vasculogenesis, these models have not previously been used to study metastasis organ specificity and investigate the role of human organ-specific microenvironments.

Here we present an organ-specific human 3D microfluidic model that enables the study of human metastatic breast cancer cell extravasation within a perfusable human microvascularized bone-mimicking (BMi) microenvironment. The resulting model represents a functional human quad-culture in which breast cancer cells flow into, adhere to, and metastasize through human microvascular networks. These networks are supported by primary human bone marrow-derived mesenchymal stem cells (hBM-MSCs) that have undergone phenotypical transition toward the smooth muscle cell lineage, embedded in a BMi microenvironment with homogeneously distributed osteo-differentiated (OD) primary hBM-MSCs.

Results

Generation of Functional 3D Microvascular Networks Within a BMi Microenvironment. We report an in vitro platform that enables the study of organ-specific human breast cancer cell extravasation into a human BMi microenvironment through a functional, perfusable 3D microvascular network. Primary hBM-MSCs were obtained from patients undergoing hip arthroplasty under written informed consent. A triculture of primary hBM-MSCs, OD primary hBM-MSCs (14-d differentiation in osteogenic medium before seeding, according to a previously optimized protocol) (26), and primary GFP-human umbilical vein endothelial cells (HUVECs) was embedded in a fibrin gel to generate a microvascular network enclosed in a BMi matrix characterized by actively secreting OD cells, which create naturally formed molecular gradients affecting both microvasculature and cancer cells. The microfluidic model used in this study consists of a microfluidic device containing a microvascular network used to conduct organ-specific extravasation experiments (Fig. 1*A*). Functional micro-vascular networks, characterized by anastomoses with the lateral media channels, were formed over 4 d (Fig. 1*B*, Fig. S1, and Movie S1), at which time, breast cancer cells were introduced, and extravasation events were monitored during the next 8 h.

Formation of functional microvascular networks within a BMi microenvironment was characterized by the expression of specific bone markers, i.e., osteocalcin and bone alkaline phosphatase (Fig. 1 *C* and *D* and Fig. S2), and vascular markers, i.e., vascular endothelial (VE)-cadherin and zonula occludens (ZO)-1 (Fig. 1 *E* and *F* and Movie S2), and α smooth muscle actin (α-SMA) (Fig. 1*G*). Primary hBM-MSCs cultured with HUVECs showed a phenotypic adaptation toward a mural cell lineage, as demonstrated by positive α-SMA immunofluorescent staining, and wrapped around patent microvessels. Furthermore, the presence of endothelial cell–cell adherens and tight junctions represents a key factor for the development of effective extravasation models: the immunofluorescent staining demonstrates the existence of mature vessel walls with well-formed cell–cell junctions. The microvascular network, characterized by complex interconnections and continuous hollow lumens (Fig. S3*A* and Movie S3), was embedded in a BMi microenvironment with primary OD hBM-MSCs secreting bone proteins such as osteocalcin and bone alkaline phosphatase (Fig. 1 *C* and *D*). We also previously demonstrated our OD primary hBM-MSCs secreted osteopontin and osteonectin and generated calcium deposits within 3D matrices (26).

Endothelial cells displayed morphological features similar to in vivo vasculatures, such as an elongated shape aligned with microvessel axes (Fig. S3*B*), in contrast to the random alignment exhibited by endothelial monolayers or endothelialized microchannels in the absence of flow (29). Finally, fluorescent microspheres (3 and 10 μm in diameter) were perfused through the system showing patent microvessels.

Cancer Cell Extravasation in a BMi Microenvironment. A perfusable microvascular network generated via a vasculogenesis-like process from endothelial cells suspended in gel solution within the microfluidic device was used to model the extravasation process of breast cancer cells toward a BMi microenvironment (Fig. 1*B* and Fig. S1). The katushka-expressing bone seeking clone (BOKL) of the MDA-MB-231 metastatic breast cancer cells flowed into the microvascular network, rolled on, and adhered to the endothelium or became physically trapped, and subsequently spread, extended filopodia through intercellular junctions into the local microenvi-ronment and finally invaded the extracellular matrix (ECM; Fig. 2 *A* and *B* and Movie S4). Cancer cells transmigrated through the endothelium into the matrices engineered to mimic three different microenvironments: bone, muscle, and acellular collagen matrix (Fig. 2*E*). Extravasation rates of the cancer cells in the BMi mi-croenvironment were significantly higher compared with the other

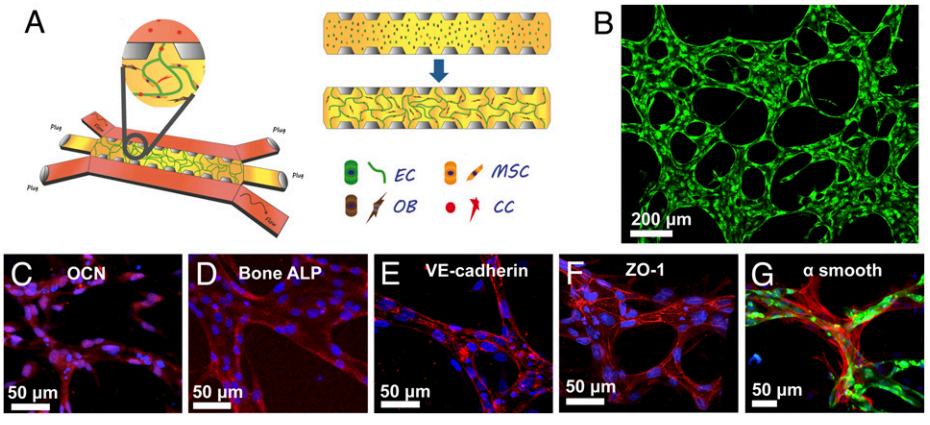

Fig. 1. Characterization of the extravasation model. (*A*) Two side media channels allow addition of cancer cells, biochemical factors, and flow across the vasculature formed in the gel channel. Endothelial cells (ECs), MSCs, and osteoblast-differentiated cells (OBs) are initially seeded in the gel. ECs form vasculature, whereas MSCs and OBs create a BMi microenvironment. Cancer cells introduced in the vessel extravasate into the organ-mimicking gel. (*B*) The microvascular network is characterized by highly branched structures. Establishment of BMi microenvironment is shown by staining for osteocalcin (OCN, red; *C*) and bone alkaline phosphatase (ALP, red; *D*), which are both secreted by OD hBM-MSCs. Formation of vasculature is confirmed by staining for endothelial adherens (VE-cadherin, red; *E*) and tight (ZO-1, red; *F*) junctions. Differentiation of hBM-MSCs to mural cell lineage when colocalized with ECs is indicated by immunofluorescent staining of α-smooth muscle actin (α-SMA, red; *G*). HUVECs (green). DAPI (nucleus, blue).

conditions such as the microenvironment conditioned with the myoblast cell line C2C12, mimicking a muscle microenvironment, or control matrix without any cells. BOKL average extravasation rate was 56.5 ± 4.8% in the presence of OD hBM-MSCs compared with 8.2 ± 2.3% with C2C12 myoblasts and 14.7 ± 3.6% without stromal cell addition (control matrix; Fig. 2*C*). The average extravasation rate within the BMi microenvironment was then 3.8-fold higher than without stromal cell addition, which is higher compared with our previous work analyzing the extravasation of cancer cells through a simple and less physiologically relevant endothelial monolayer (2.06). It is noteworthy that the presence of actively secreting mural cell-like hBM-MSCs that enabled the generation of a more in vivo-like microenvironment could have also played a role in the increased extravasation ratio. No significant differences were quantified comparing cancer cell migration distance following extravasation in BMi microenvironments and control matrices (23.26 ± 2.73 vs. 30.63 ± 6.07 μm).

Vessel permeability was quantified by analyzing 70-kDa dextran diffusion through the microvascular wall and compared among experimental conditions (Fig. S3*A*). Permeability values were significantly higher in BMi microfluidic devices $4.12 \times 10^{-6} \pm 0.75 \times 10^{-6}$ cm/s compared with control matrices $0.89 \times 10^{-6} \pm 0.31 \times 10^{-6}$ cm/s (Fig. 2*D*). Finally, the highest permeability values were found in the presence of C2C12 myoblasts $8.37 \times 10^{-6} \pm 1.53 \times 10^{-6}$ cm/s, resulting in a 2.0-fold increase compared with the BMi systems (Fig. 2*D*). It is surprising that the most leaky environment C2C12 gave rise to the lowest extravasation rate. This demonstrates that permeability is only one of multiple factors affecting extravasation.

We also explored the capability of the assay to distinguish between the extravasation potentials of different cell types and cellular environments. First, an inflammatory model was set up with the addition of a macrophage cell line. RAW264.7 macrophages were homogeneously dispersed within the fibrin gel. The average extravasation rate within macrophage conditioned BMi microenvironment was significantly higher (32.4 ± 4.3%) compared with matrices without addition of stromal cells (14.7 ± 3.6%) but lower with respect to standard BMi microenvironment (56.5 ± 4.8%; Fig. S4*A*). The promising nature of these data were confirmed by microvessel permeability values, which were higher ($6.77 \times 10^{-6} \pm 1.56 \times 10^{-6}$ cm/s) in presence of macrophages compared with BMi matrices ($4.12 \times 10^{-6} \pm 0.75 \times 10^{-6}$ cm/s; Fig. S4*B*). We also performed a control experiment introducing nonmetastatic mammary epithelial cells (MCF-10A) within the BMi microenvironment. MCF-10A extravasation rate was significantly lower (5.2 ± 2.5%) compared with BOKL (56.5 ± 4.8%; Fig. S5), thus demonstrating the specificity of the interaction between metastatic cancer cells and a BMi microenvironment.

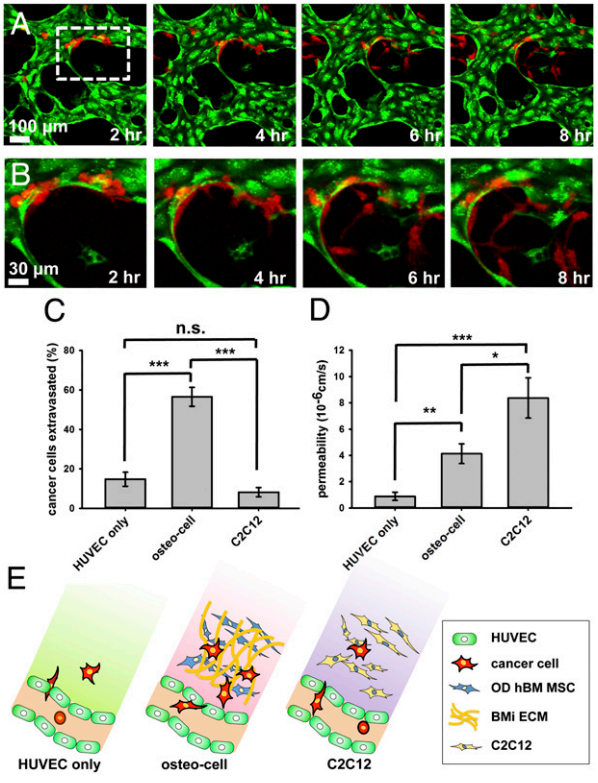

Fig. 2. Cancer cell extravasation. (*A*) Extravasation of cancer cells (red) introduced into the vascular network (HUVECs, green) is monitored in real time. (*B*) Magnified images of white dotted box in *A* show extravasation of cancer cells. (*C*) Percent of cancer cells extravasated varies significantly among the vascular networks embedded in different microenvironments, i.e., acellular and bone or muscle-mimicking microenvironment, respectively. (*D*) Permeability values increased when cells are added to mimic the two organ-specific microenvironments compared with HUVEC only condition. (*E*) Schematic of HUVEC only, osteo-cell, and C2C12 cell added systems. HUVECs are shown as green cells that form vessel, osteo-cells are blue colored cells and secrete bone matrix as shown in yellow, and C2C12 cells are depicted as yellow cells. Cancer cells are colored in red and seen both in the vessels as well as extravasated out in the surrounding matrix.

The Role of Adenosine in Cancer Cell Extravasation. As we found striking differences between cancer cell extravasation within BMi and muscle-mimicking microenvironments, we asked which factors secreted by muscle might be responsible. It is reported that the skeletal muscle microenvironment reduces cancer cell tumorigenicity and elicits paracrine-mediated cytotoxic and cytostatic responses from metastatic cancer cells (30). In particular, several studies identified the A_3 adenosine receptor (A_3AR), which is expressed by multiple cancer cell types (31), as key in the antimetastatic and protective effect of skeletal muscle cells (32). Before investigating the role of A_3AR in extravasation, we first demonstrated through immunofluorescence that BOKL introduced in our system expressed the A_3AR (Fig. 3*A* and Fig. S6). Then, we introduced the A_3AR antagonist PSB-10 within C2C12 containing microfluidic devices (Fig. 3*H*) and preincubated cancer cells with A_3AR before seeding (33). With the addition of the antagonist, cancer cell extravasation rate significantly increased (32.4 ± 7.7%) compared with nontreated C2C12 matrices (8.2 ± 2.3%; Fig. 3*E*), whereas microvessel permeability was not significantly affected ($7.4 \times 10^{-6} \pm 2.61 \times 10^{-6}$ vs. $8.04 \times 10^{-6} \pm 1.72 \times 10^{-6}$ cm/s; Fig. 3*G*). These data indirectly demonstrate the presence of C2C12-secreted adenosine in the system, as well as the protective role of this molecule against cancer metastases. Mass spectrometry (MS) analyses performed on cell culture supernatants provided further evidence of adenosine secretion by the C2C12-conditioned microenvironment (Fig. 3*B* and Fig. S7), whereas immunofluorescence staining demonstrated the expression of the adenosine converter CD73 (Fig. 3*C*), which catalyzes the conversion of AMP to adenosine (34).

Supported by our results with untreated or conditioned (A_3AR antagonist) C2C12 microenvironments, we investigated the role of adenosine on cancer cell extravasation within a BMi microenvironment using our model as drug screening platform (Fig. 3*H*). The presence of adenosine significantly reduced cancer cell extravasation (12.7 ± 2.8%) compared with the untreated BMi microenvironment (56.5 ± 4.8%; Fig. 3*D*). Furthermore, we found a dramatic increase in microvasculature permeability ($8.22 \times 10^{-6} \pm 1.76 \times 10^{-6}$ cm/s) compared with BMi control ($4.12 \times 10^{-6} \pm 0.75 \times 10^{-6}$ cm/s; Fig. 3*F*). It is interesting to note that treating BMi microenvironments with adenosine led to extravasation rate and permeability values comparable to C2C12-conditioned matrices, suggesting this molecule could be theoretically used to tune a specific microenvironment with antimetastatic

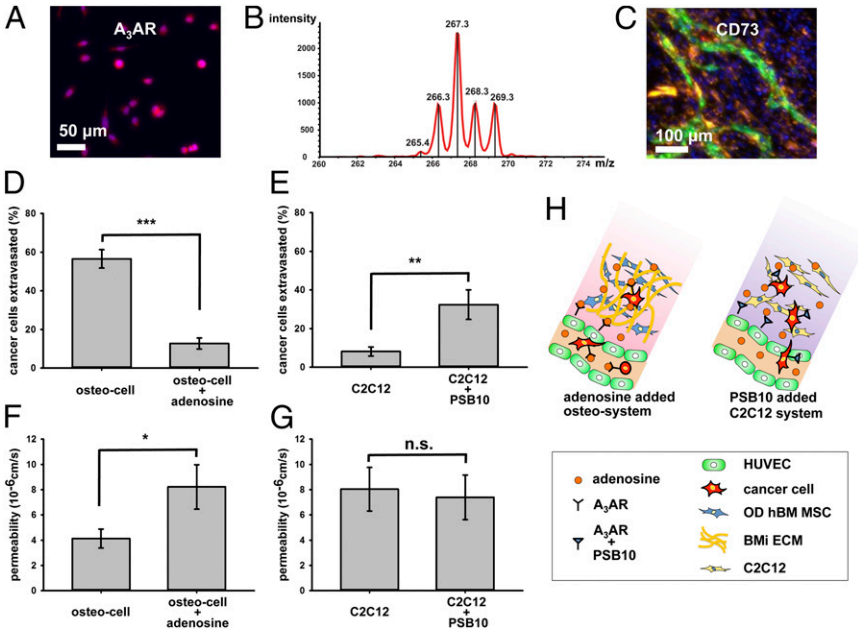

Fig. 3. Percent of cancer cell extravasation and vascular permeability in bone and muscle-mimicking microenvironment with addition of stimulating or blocking molecules. Cancer cells express the A_3 adenosine receptor (*A*), whereas C2C12 embedded matrices secrete adenosine as shown by MS data (268 *m/z* peak) (*B*) and CD73 immunofluorescent staining (*C*). Percentage of cancer cells that extravasate (*D*) and permeability of the vasculature (*F*) in the BMi microenvironment with OD hBM-MSCSs, with and without adenosine. Extravasation rate decreased significantly with addition of adenosine, whereas the permeability increased with adenosine. Percentage of cancer cells that extravasate (*E*) and permeability of the vasculature (*G*) in the muscle-mimicking microenvironment with C2C12 cells, with and without PSB10. Although blocking of A_3AR with the addition of PSB10 did not alter the permeability of the vasculature, cancer cell extravasation rate increased significantly. (*H*) Schematic of osteo-cell and C2C12 cell added systems with adenosine, A_3 adenosine receptor and its antagonist PSB10.

properties. Finally, Live/Dead and MTT assays were performed at different time points on cancer cells treated with adenosine, confirming that the A_3AR antagonist action in reducing extravasation was not due to a cytotoxic effect on BOKL (Figs. S8 and S9).

Effect of Shear Stress on Microvasculature and Cancer Cell Extravasation. Because extravasation normally occurs during blood flow, we next examined the effects on microvascular networks conditioned by physiological levels of shear stress. In these experiments, we preconditioned microvascular networks with flow overnight before cancer cell seeding and analyzed the effects of flow on extravasation and microvessel permeability. We selected a flow rate of 2 μL/min in the channel, which resulted in an average velocity in the vasculature of 220 μm/s and a wall shear stress of 0.25 dyne/cm^2 (35).

Cancer cell extravasation within the flow conditioned BMi microenvironment occurred at a rate of 38.6 ± 4.8% (Fig. 4*A*), significantly lower than under static conditions (56.5 ± 4.8%). We also found that microvessel permeability decreased 2.4-fold compared with static conditions ($1.72 \times 10^{-6} \pm 0.53 \times 10^{-6}$ cm/s compared with $4.12 \times 10^{-6} \pm 0.75 \times 10^{-6}$ 10^{-6} cm/s; Fig. 4*B*). Endothelial cells exposed to a laminar flow were characterized by an elongated morphology and a clear actin filament alignment in the flow direction as shown in Fig. 4 *E* (flow) and *D* (static control) and measured using anisotropy score (Fig. S10 and *SI Materials and Methods*), with compelling stress fibers at cell–cell junctions (Fig. S3*B*), thus displaying morphological features resembling in vivo microvessels (36). Finally, it is worth noting that flow-conditioned breast cancer cells migrated further into the surrounding matrix (33.7 ± 4.3 μm) compared with static experiments (23.3 ± 2.7 μm; Fig. 4*C*).

Discussion

An organ-specific 3D microfluidic model was created to study human breast cancer cell extravasation into an actively secreting BMi microenvironment generated with OD hBM-MSCs through perfusable human microvascular networks composed of endothelial and mural-like cells. The relevance of the present work lies in the application of a complex model to investigate and subsequently tune a specific step of the metastatic cascade within different organ-specific microenvironments with implications for the screening of new therapeutics. The efficacy and potentiality of our microfluidic model go beyond the established role of adenosine as a promising anticancer molecule to specifically demonstrate its involvement in the extravasation process.

The microfluidic model presented is based on the coculture of endothelial and hBM-MSC–derived mural cells to create physiologically relevant highly branched structures, characterized by reduced microvessel diameter and increased branch number compared with microvascular networks made of endothelial cell alone (27). Particularly, this model overcomes some of the limitations of previously developed elegant models that showed impaired perfusability when supportive stromal cells were added to the system (37). It is known that a wide panel of molecules is involved in vessel wall and network maturation including vascular endothelial growth factor (VEGF), platelet derived growth factor (PDGF-B), and members of the TGF-β family. Moreover, it is reported that angiopoietin-1 (Ang-1) represents a key

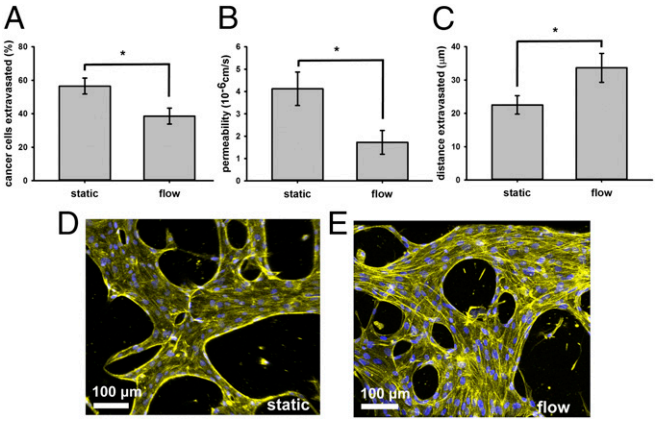

Fig. 4. Cancer cell extravasation and endothelial cell (EC) permeability change in the presence of flow through the vasculature. Extravasation of cancer cells (*A*) and permeability of the vasculature (*B*) decreased significantly with the addition of flow. (*C*) Extravasated cancer cells migrated further in the flow condition vs. the static condition. Actin (yellow) within ECs in static condition (*D*) and under conditions when flow was added in the vasculature (*E*). DAPI (nucleus, blue).

molecule in vessel stabilization and could play a role in the recruitment of mesenchymal cells (38). As we recently demonstrated, the addition of Ang-1 within HUVEC + hBM-MSC cocultures significantly induces mesenchymal cell expression of common markers displayed by mural cells, e.g., α-SMA, SM22α, and NG-2 (27), which contribute to network stabilization. Taken together, these findings provide evidence that the combination of endothelial-mesenchymal stem cell coculture and the external addition of stabilizing molecules promote the generation of functional microvascular networks, which represent a suitable model to study cancer cell extravasation within an actively secreting BMi microenvironment.

Cancer cell extravasation rates were significantly higher in the BMi microenvironment compared with control matrices without stromal cells or muscle-mimicking microenvironments. Although the higher permeability in the BMi microenvironment is likely due to a combination of factors, it may also contribute to the increase in extravasation. Indeed, matrix-specific cell-secreted chemokines can both generate molecular gradients affecting cancer cell transendothelial migration (39) and alter endothelial permeability (40). Of particular note is the increase in microvasculature permeability when adenosine is added. It has been reported that adenosine can interact with endothelial cells expressing A_2B adenosine receptors, promoting the release of proangiogenic factors including VEGF and IL-8, which could lead to the increased permeability (41). Although A_2B adenosine receptors are preferentially expressed by human microvascular endothelial cells compared with HUVECs, the external addition of adenosine in the BMi microenvironment played a role in the increased microvessel permeability compared with untreated matrices, despite reducing cancer cell extravasation. These data highlight that permeability represents only one of the key factors driving cancer cell extravasation. C2C12-secreted adenosine could also partially explain permeability differences detected comparing no stromal cell addition, BMi microenvironment, and C2C12 conditioned matrices. Moreover, the presence of high values of microvessel permeability with the addition of the A_3AR antagonist within C2C12-embedded microenvironments, which are comparable to data obtained with untreated C2C12 matrices, suggests the A_3AR antagonist did not adversely affect the mechanical properties of the endothelium, confirming previous studies demonstrating low expression levels of A_3AR by endothelial cells (41). However, the addition of the antagonist did promote an increase in the extravasation rate compared with untreated microenvironments, suggesting a specific interaction with cancer cells. Indeed, it should also be considered the A_3AR antagonist could have affected endothelial cell secretory activity or the expression of surface markers contributing to cancer cell adhesion/extravasation, thus leading to increased extravasation rates.

Substantial clinical and experimental evidence indicates a key role of macrophages in multiple steps of the metastatic cascade. Based on previous experiments performed in our laboratory on cancer cell intravasation (20), we suggest the increased microvasculature permeability could be due to the macrophage secretion of the inflammatory cytokine TNF-α. However, it is known that TNF-α inhibits osteoblast differentiation and bone-specific protein expression, particularly osteocalcin, while inducing osteoclastogenesis (42). Then, we can speculate the macrophage-secreted TNF-α could have conditioned the BMi microenvironment, limiting the prometastatic effect induced by OD cell secretome. Further analyses are required to in-depth investigate specific role and impact of macrophages and particularly macrophage-secreted TNF-α on breast cancer bone metastases.

Several works have recently shown that when endothelial cells are subjected to laminar flow shear stress, transendothelial electrical resistance increases, microvasculature permeability decreases, actin filaments become more aligned, and cytoskeletal tension and intercellular forces between endothelial cells increase compared with static conditions. Moreover, a significant overexpression has been highlighted for β-catenin (adherens junctions) and ZO-1 (tight junctions), with respect to disturbed flow or static conditions (43). Overall, these studies suggest that exposure of endothelial cells to controlled, laminar flows results in cell–cell junction tightening with a corresponding decrease in vasculature permeability. These findings agree with our results showing decreased microvessel permeability due to flow shear stress in the same BMi microenvironment. It is likely that the reduced extravasation rate within the flow conditioned BMi microenvironment could be due to enhanced endothelial cell intercellular forces and cell–cell junction tightening. Furthermore, we can speculate the presence of an interstitial flow within the BMi matrix during flow conditioned experiments could partially explain the increased migration distance shown by breast cancer cells compared with static controls, as previously demonstrated by several studies highlighting the link between flow-induced mechanical stimulation and cell migration (21). Our data demonstrate that generation of a more physiological microenvironment with the addition of endothelial wall shear stress can dramatically affect extravasation potential, which could have critical implications on drug screening tests and in vitro model development. We would like to emphasize that, in addition to endothelial cell preconditioning, our platform enables real time monitoring of cancer cell extravasation under flow, thus allowing the in situ analysis of extravasation in the microenvironment where both endothelial and cancer cells are exposed to physiological stimuli.

In conclusion, an organ-specific vascularized 3D microfluidic model was created to study human breast cancer cell extravasation into an actively secreting human BMi microenvironment through perfusable human microvascular networks composed of endothelial and mural-like cells. We found clear evidence of the seed (breast cancer cells) and soil (BMi microenvironment) coupling and provided quantitative results regarding the antimetastatic and protective role played by skeletal muscle cells. Particularly, we demonstrated the effectiveness of the model as a drug screening assay, being able to investigate both the effects of A_3AR antagonist on cancer cell extravasation in a C2C12 myoblast conditioned matrix and the antimetastatic role of adenosine in a human BMi microenvironment, thus overcoming limitations of traditional in vitro models. These assays contribute to the continued evolution of 3D in vitro models, improving on drawbacks of animal studies, e.g., differences in drug metabolism that affect the outcome of therapeutic treatments, and capable of bridging highly specific human in vitro cultures with physiological in vivo conditions. Success in these modeling efforts will help to foster a more effective screening of tailored anticancer therapies in the context of personalized medicine and promote the study of key molecular pathways involved in cancer biology in controlled, organ-specific, physiological-like conditions.

Materials and Methods

Microfluidic System. The microfluidic system contains a 1.3-mm-wide central hydrogel region flanked by two lateral media channels, as previously used in our group for other studies (27). The microfabrication process of the device was documented in detail for other configurations (26). Briefly, the microfluidic device was fabricated with poly-dimethyl-siloxane (PDMS, Silgard 184; Dow Chemical) using soft lithography techniques from patterned SU-8 silicon wafers. Inlet and outlet ports were created with biopsy punches, and a cover glass was bonded to the PDMS after 60-s oxygen plasma treatment to generate 200-μm-deep microchannels. A thrombin solution (4 U/mL) was used to resuspend cells, and 10-μL aliquots were mixed with 10 μL fibrinogen solution (5 mg/mL) to create a fibrin gel. After gelation, media channels were filled with cell culture medium, and microfluidic devices were cultured for 4 d. The two channels system enabled easy access to the hydrogel region for cancer cell extravasation studies under static or dynamic conditions.

Immunofluorescent Staining and Image Acquisition. All devices were washed with PBS (Invitrogen), fixed with 4% paraformaldehyde (PFA) for 15 min and permeabilized with 0.1% Triton-X 100 solution for 5 min at room temperature. Samples were treated with 5% BSA + 3% (wt/vol) goat serum solution for at least 3 h at 4 °C before incubation with primary antibody. Mouse polyclonal α-SMA antibody (abcam; dilution 1:100), rabbit polyclonal VE-cadherin antibody (abcam; dilution 1:100), mouse polyclonal ZO-1 antibody (Invitrogen; dilution 1:100), rabbit polyclonal osteocalcin antibody (BTI; dilution 1:50), and mouse monoclonal bone alkaline phosphatase (abcam; dilution 1:40) were used for staining. Red fluorescently labeled secondary antibodies (Invitrogen) were used at 1:200 dilution (Invitrogen). Cell nuclei were stained with DAPI (5 mg/mL; Invitrogen) at 1:500 dilution, and F-actin filaments were stained with AlexaFluor633 phalloidin (Invitrogen) at 1:100 dilution. All images were captured using a confocal microscope (Olympus IX81) and processed with Imaris software (Bitplane Scientific Software).

Addition of Adenosine and Antagonist for the Adenosine Receptor. Additional experiments were performed to test the role of the muscle-secreted molecule adenosine as an antimetastatic agent. Adenosine (R&D Systems) was diluted at a final concentration of 10 μM and added to BMi microfluidic devices for 24 h before cancer cell addition. Cancer cells were preincubated with adenosine 4 h before the seeding. Extravasation events were monitored in presence of adenosine. To confirm the presence and effect of adenosine within C2C12 myoblast conditioned matrices, the highly specific A_3AR antagonist (PSB-10; R&D Systems) at 10 μM was introduced into the microfluidic devices for 24 h before cancer cell addition, and cancer cells were preincubated with A_3AR for 4 h before injection. Extravasation events were monitored in presence of A_3AR antagonist.

Statistics. All extravasation percentages are reported as averages ± standard error of the mean (SEM). Measurements are obtained from a minimum of 10 regions of interest (ROIs) from three or more independent devices, whereas all permeability values are averages of five (minimum) to seven (maximum) measurements from two (minimum) to four (maximum) independent devices. Measurements were compared using an unpaired Student *t* test. Statistical tests were performed with SigmaPlot12. All tests with $P < 0.05$ and $P < 0.005$ were assumed to be statistically significant.

ACKNOWLEDGMENTS. We thank Prof. Andrea Mele and Walter Panzeri (Politecnico di Milano) for MS experiments and support during data analysis. This work as supported by National Cancer Institute Grants R33 CA174550-01 and R21 CA140096 and the Italian Ministry of Health. S.B. was supported by the Fondazione Fratelli Agostino and Enrico Rocca through a Progetto Rocca doctoral fellowship, and J.S.J. was supported by a Draper fellowship.

1. Valastyan S, Weinberg RA (2011) Tumor metastasis: Molecular insights and evolving paradigms. *Cell* 147(2):275–292.
2. Chambers AF, Groom AC, MacDonald IC (2002) Dissemination and growth of cancer cells in metastatic sites. *Nat Rev Cancer* 2(8):563–572.
3. Hanahan D, Weinberg RA (2011) Hallmarks of cancer: The next generation. *Cell* 144(5):646–674.
4. Fidler IJ (2003) The pathogenesis of cancer metastasis: The 'seed and soil' hypothesis revisited. *Nat Rev Cancer* 3(6):453–458.
5. Bussard KM, Gay CV, Mastro AM (2008) The bone microenvironment in metastasis: What is special about bone? *Cancer Metastasis Rev* 27(1):41–55.
6. Coleman RE (2012) Bone cancer in 2011: Prevention and treatment of bone metastases. *Nat Rev Clin Oncol* 9(2):76–78.
7. Kim MY, et al. (2009) Tumor self-seeding by circulating cancer cells. *Cell* 139(7):1315–1326.
8. Nguyen DX, Bos PD, Massagué J (2009) Metastasis: From dissemination to organ-specific colonization. *Nat Rev Cancer* 9(4):274–284.
9. Reymond N, d'Água BB, Ridley AJ (2013) Crossing the endothelial barrier during metastasis. *Nat Rev Cancer* 13(12):858–870.
10. Al-Mehdi AB, et al. (2000) Intravascular origin of metastasis from the proliferation of endothelium-attached tumor cells: A new model for metastasis. *Nat Med* 6(1): 100–102.
11. Stoletov K, et al. (2010) Visualizing extravasation dynamics of metastatic tumor cells. *J Cell Sci* 123(Pt 13):2332–2341.
12. Schumacher D, Strilic B, Sivaraj KK, Wettschureck N, Offermanns S (2013) Platelet-derived nucleotides promote tumor-cell transendothelial migration and metastasis via P2Y2 receptor. *Cancer Cell* 24(1):130–137.
13. Kuperwasser C, et al. (2005) A mouse model of human breast cancer metastasis to human bone. *Cancer Res* 65(14):6130–6138.
14. Lauffenburger DA, Horwitz AF (1996) Cell migration: A physically integrated molecular process. *Cell* 84(3):359–369.
15. Simpson KJ, et al. (2008) Identification of genes that regulate epithelial cell migration using an siRNA screening approach. *Nat Cell Biol* 10(9):1027–1038.
16. Bersini S, Jeon JS, Moretti M, Kamm RD (2014) In vitro models of the metastatic cascade: From local invasion to extravasation. *Drug Discov Today* 19(6):735–742.
17. Shin Y, et al. (2012) Microfluidic assay for simultaneous culture of multiple cell types on surfaces or within hydrogels. *Nat Protoc* 7(7):1247–1259.
18. Vickerman V, Kamm RD (2012) Mechanism of a flow-gated angiogenesis switch: Early signaling events at cell-matrix and cell-cell junctions. *Integr Biol (Camb)* 4(8):863–874.
19. Sung KE, et al. (2011) Transition to invasion in breast cancer: A microfluidic in vitro model enables examination of spatial and temporal effects. *Integr Biol (Camb)* 3(4): 439–450.
20. Zervantonakis IK, et al. (2012) Three-dimensional microfluidic model for tumor cell intravasation and endothelial barrier function. *Proc Natl Acad Sci USA* 109(34): 13515–13520.
21. Polacheck WJ, Charest JL, Kamm RD (2011) Interstitial flow influences direction of tumor cell migration through competing mechanisms. *Proc Natl Acad Sci USA* 108(27): 11115–11120.
22. Pathak A, Kumar S (2012) Independent regulation of tumor cell migration by matrix stiffness and confinement. *Proc Natl Acad Sci USA* 109(26):10334–10339.
23. Song JW, et al. (2009) Microfluidic endothelium for studying the intravascular adhesion of metastatic breast cancer cells. *PLoS ONE* 4(6):e5756.
24. Jeon JS, Zervantonakis IK, Chung S, Kamm RD, Charest JL (2013) In vitro model of tumor cell extravasation. *PLoS ONE* 8(2):e56910.
25. Zhang Q, Liu T, Qin J (2012) A microfluidic-based device for study of transendothelial invasion of tumor aggregates in realtime. *Lab Chip* 12(16):2837–2842.
26. Bersini S, et al. (2014) A microfluidic 3D in vitro model for specificity of breast cancer metastasis to bone. *Biomaterials* 35(8):2454–2461.
27. Jeon JS, et al. (2014) Generation of 3D functional microvascular networks with human mesenchymal stem cells in microfluidic systems. *Integr Biol (Camb)* 6(5):555–563.
28. Moya ML, Hsu YH, Lee AP, Hughes CC, George SC (2013) In vitro perfused human capillary networks. *Tissue Eng Part C Methods* 19(9):730–737.
29. Chrobak KM, Potter DR, Tien J (2006) Formation of perfused, functional microvascular tubes in vitro. *Microvasc Res* 71(3):185–196.
30. Parlakian A, et al. (2010) Skeletal muscle phenotypically converts and selectively inhibits metastatic cells in mice. *PLoS ONE* 5(2):e9299.
31. Madi L, et al. (2004) The A3 adenosine receptor is highly expressed in tumor versus normal cells: Potential target for tumor growth inhibition. *Clin Cancer Res* 10(13): 4472–4479.
32. Fishman P, et al. (2004) An agonist to the A3 adenosine receptor inhibits colon carcinoma growth in mice via modulation of GSK-3 beta and NF-kappa B. *Oncogene* 23(14):2465–2471.
33. Müller CE (2003) Medicinal chemistry of adenosine A3 receptor ligands. *Curr Top Med Chem* 3(4):445–462.
34. Regateiro FS, Cobbold SP, Waldmann H (2013) CD73 and adenosine generation in the creation of regulatory microenvironments. *Clin Exp Immunol* 171(1):1–7.
35. Evani SJ, Prabhu RG, Gnanaruban V, Finol EA, Ramasubramanian AK (2013) Monocytes mediate metastatic breast tumor cell adhesion to endothelium under flow. *FASEB J* 27(8):3017–3029.
36. He P, Adamson RH (1995) Visualization of endothelial clefts and nuclei in living microvessels with combined reflectance and fluorescence confocal microscopy. *Microcirculation* 2(3):267–276.
37. Kim S, Lee H, Chung M, Jeon NL (2013) Engineering of functional, perfusable 3D microvascular networks on a chip. *Lab Chip* 13(8):1489–1500.
38. Jain RK (2003) Molecular regulation of vessel maturation. *Nat Med* 9(6):685–693.
39. Hsu YL, Hou MF, Kuo PL, Huang YF, Tsai EM (2013) Breast tumor-associated osteoblast-derived CXCL5 increases cancer progression by ERK/MSK1/Elk-1/snail signaling pathway. *Oncogene* 32(37):4436–4447.
40. Borsig L, Wolf MJ, Roblek M, Lorentzen A, Heikenwalder M (2014) Inflammatory chemokines and metastasis—tracing the accessory. *Oncogene* 33(25):3217–3224.
41. Feoktistov I, et al. (2002) Differential expression of adenosine receptors in human endothelial cells: Role of A2B receptors in angiogenic factor regulation. *Circ Res* 90(5): 531–538.
42. Abbas S, Zhang YH, Clohisy JC, Abu-Amer Y (2003) Tumor necrosis factor-alpha inhibits pre-osteoblast differentiation through its type-1 receptor. *Cytokine* 22(1-2): 33–41.
43. Colgan OC, et al. (2007) Regulation of bovine brain microvascular endothelial tight junction assembly and barrier function by laminar shear stress. *Am J Physiol Heart Circ Physiol* 292(6):H3190–H3197.